Brain Tissue Segmentation Approach: Combining Gaussian Mixture Models with Atlas-based and Tissue-Model Methods

Mahdi Islam[1] and Musarrat Tabassum[1]

[1] *University of Girona, Erasmus Mundus Joint Master's Program in Medical Imaging and Applications (MAIA).*

November 20, 2024

Abstract

Accurate and timely diagnosis of neurological conditions is critical for effective treatment and improving patient outcomes. Brain tissue segmentation plays a pivotal role in neurological research by enabling detailed analysis of brain structure and function. In medical imaging, precise segmentation of brain tissues is essential for accurate diagnosis and treatment planning, contributing to advancements in understanding the brain. This study combines two widely utilized techniques in brain tissue segmentation: the Gaussian Mixture Model and the Probabilistic Atlas. By exploring multiple initialization strategies, independent segmentation processes, and different atlas types, the approach evaluates segmentation performance under varying conditions. Results indicate that integrating a Gaussian mixture model with an atlas constructed from images acquired using the same scanner and patient demographic enhances segmentation accuracy. However, this may come at the cost of reduced generalizability across diverse datasets.

Keywords—Brain tissue segmentation, Probabilistic Brain Atlas, Tissue Probability Models, Expectation Maximization (EM), Gaussian Mixture Models (GMM), Magnetic Resonance Imaging (MRI)

1 Introduction

Medical image segmentation is an important part of medical imaging that helps identify and separate different parts of the body in medical scans. This is especially useful for diagnosing and planning treatments for patients. For example, in brain scans like magnetic resonance (MR) images, segmentation helps divide the brain into areas like grey matter (GM), white matter (WM), and cerebrospinal fluid (CSF). This process looks at features like intensity, texture, and uniformity to classify these brain regions accurately. There are many ways to perform segmentation, including methods that use labeled data (supervised) and those that do not (unsupervised). Clustering is one of the most common techniques because it is simple and works well. In this study, we explore different segmentation methods such as clustering, probabilistic atlases, tissue models, and maps based on intensity information. The goal is to compare these methods, understand their strengths, and improve the accuracy of brain tissue segmentation, which can lead to better tools for medical imaging.

2 Dataset

The dataset contains 20 T1-weighted scan and ground truth of segmentation masks for each cases that corresponds to white matter (WM), grey matter (GM), and cerebrospinal fluid (CSF). Figure 01 shows the images of the dataset.

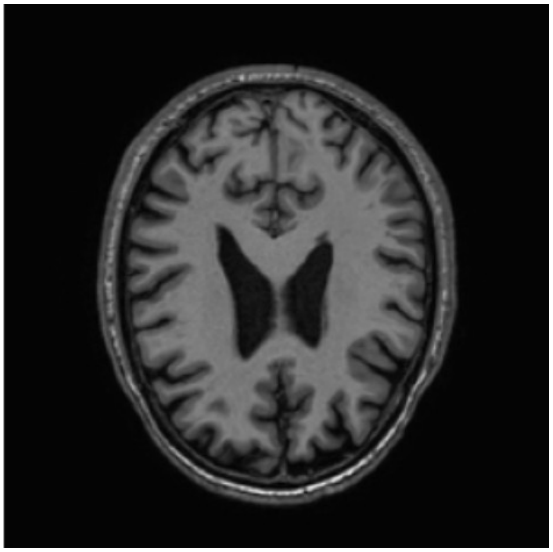

(a) T1-weighted MRI scan

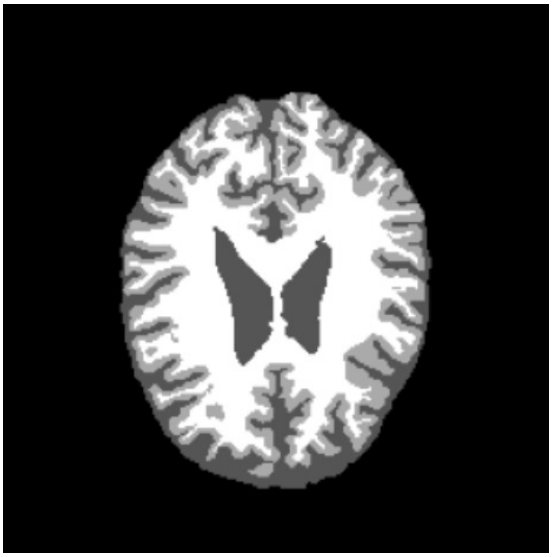

(b) Corresponding ground truth

Figure 1: Dataset showing T1-weighted MRI scans and corresponding ground truth. (a) T1-weighted MRI scan. (b) Ground truth.

3 Methodology

The methodology is divided into three main subsections; Atlas Registration, Segmentation without Gaussian Mixture Models(GMM) and Segmentation with GMM.

3.1 Registration

3.1.1 Atlas Registration

The first step in the segmentation process was to register the atlas, which represents the mean image, with the target. To achieve this, both affine and B-spline registration techniques were employed. For the affine registration, the transform was initialized using the center of gravity method, and the process utilized an advanced Mattes Mutual Information metric with an adaptive stochastic gradient descent optimizer. The registration was conducted in four resolutions, and the maximum number of iterations per resolution was set to 1000.

For the B-spline registration, the localized Mattes Mutual Information metric was used, optimized with a standard gradient descent approach. This method included a multi-resolution pyramid with a final grid spacing of 15 mm and a grid spacing schedule of [4, 4, 2, 1]. The registration parameters were fine-tuned for efficiency by employing random coordinate sampling with a sample region size of $50 \times 50 \times 50$ mm and using 2000 spatial samples per resolution.

To identify the target image for registration, the mean intensity score and histogram score of all images in the dataset were calculated and combined. The image with the minimum combined score was selected as the target. All parameter files used for registration are accessible in the ModelZoo repository. The registrations were performed using itk-elastix.

3.1.2 Label Propagation

To create the probabilistic atlas, we needed to apply the previously computed registration to the labels of each of the images in the dataset. Using the transformation matrices obtained in the previous section, in this step we transformed each of the label images separately. This is done to prevent any overlap or interpolation errors between the labels.

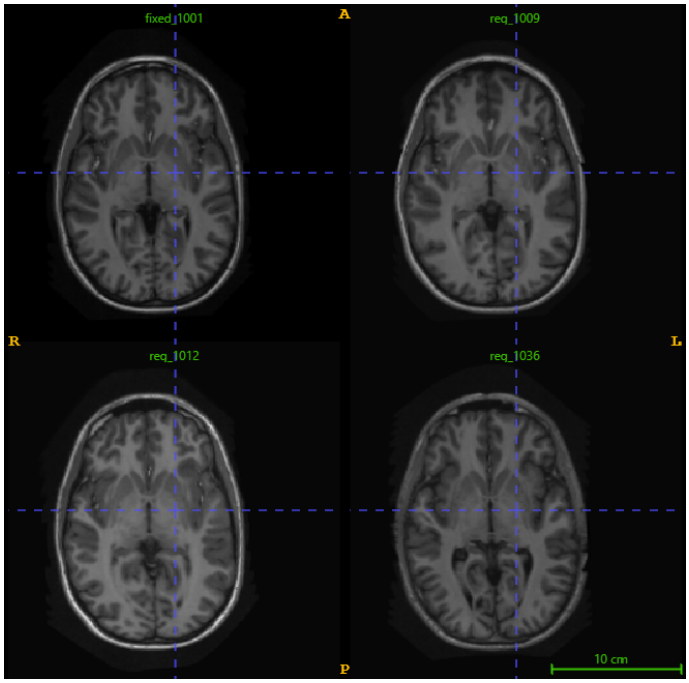

Figure 2: Samples of registered images.

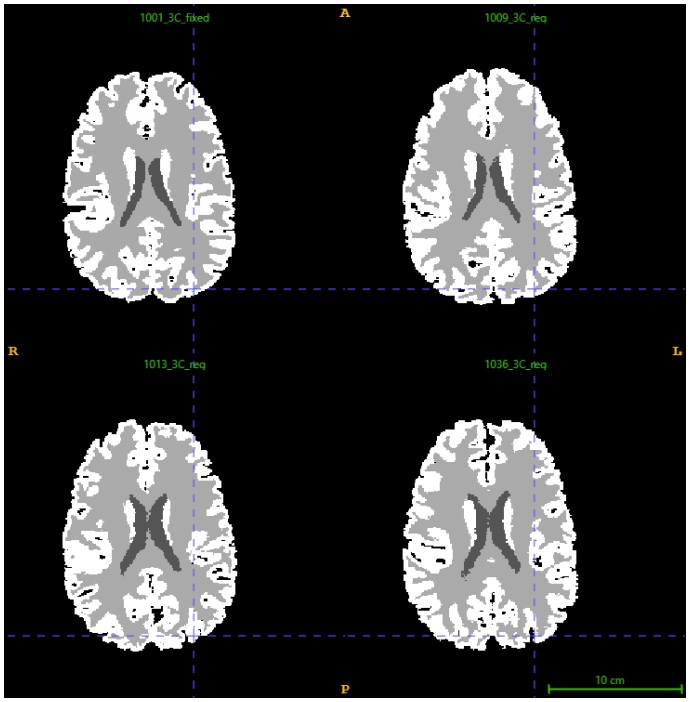

Figure 3: Samples of registered masks.

3.1.3 Mean Image and Probabilistic Atlas

- After the label propagation is carried out, we construct our probabilistic brain atlas by computing the voxel-wise mean across all propagated labels of each image, treating each label distinctly.

- Atemplate or mean image is commonly used for registration or analysis options at later point. In order to compute this image, the voxel-wise mean of the registered moving images and the fixed image are taken.

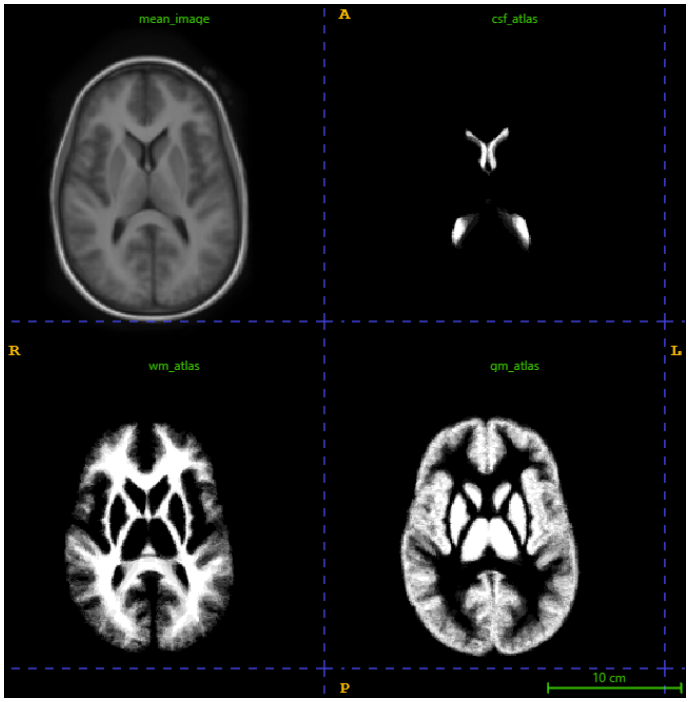

Figure 4: Mean Image and Probabilistic Atlas.

3.2 Tissue Models

Thetissue probabilistic model is a strategy in which the voxel intensity information of each of the images in our dataset is translated into a map of tissue probabilities. This map will provide us with the probability of a given intensity value be longing to each of the tissue labels. To compute this model, we have followed the next steps:

- To build tissue models, we first extracted intensity profiles by applying ground truth masks to the images, isolating intensity values for white matter (WM), grey matter (GM), and cerebrospinal fluid (CSF). The intensities were normalized to a [0, 255] range using Min-Max normalization to ensure consistency across images, and histograms were created for each tissue type to map the intensity distributions.

- Subsequently, histograms were normalized to scale the values within each class and transformed into probability distributions by ensuring the total probabilities summed to one. To smooth these distributions and reduce sharp peaks, a Gaussian filter (sigma = 20) was applied, creating refined tissue probability histograms. The resulting data, representing probabilities for each tissue type across intensity values, was saved in a CSV file for further analysis.

3.3 Segmentation without GMM

3.3.1 Segmentation using Tissue Models

Among the various segmentation methods tested in this experiment, tissue model segmentation was the primary choice. This approach relies solely on voxel intensity data for segmentation, thereby excluding spatial information from the images. Previously, we computed a 256×3 matrix (the Tissue Models Probabilities), where 256 represents the probability of the normalized intensity values of the images, and 3 corresponds to the brain's tissue types. For segmentation, values 1, 2, and 3 were assigned to WM, GM, and CSF, respectively, for each intensity level in the range $[0, 255]$, based on the highest probability across the three tissue types. The formula used is as follows:

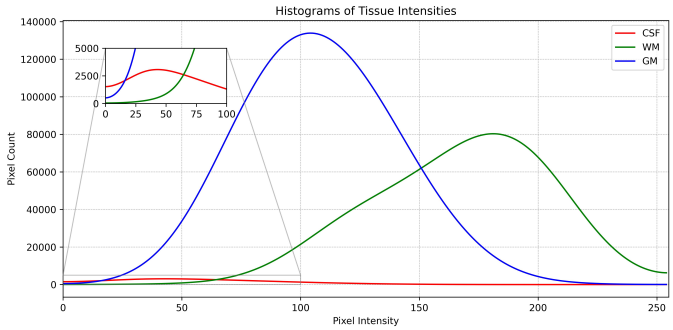

(a) Intensity distribution of the different tissues in the dataset.

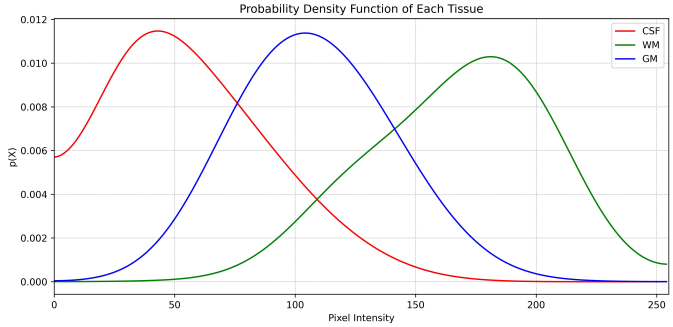

(b) Normalized intensity distribution of the different tissues in the dataset.

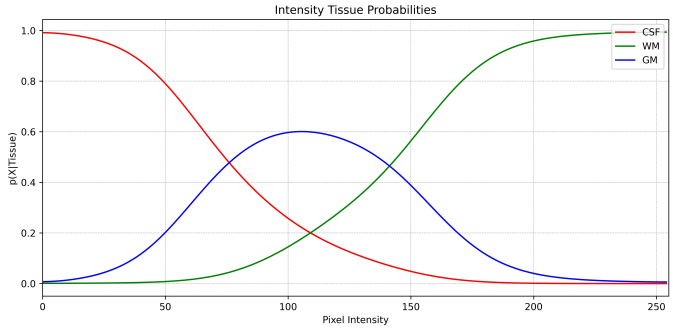

(c) Tissue probability.

Figure 5: Tissue Models

$$\text{TissueModel} = \arg \max_{j \in \{0,1,2\}} \text{Prob}[i,j] \quad \text{for } i = 0, 1, \ldots, 255 \tag{1}$$

After computing the highest probability across the three tissue types, we used this information to change each pixel intensity value of the original image to the corresponding value of the tissue model. As a result, an image segmented into WM, GM, and CSF is obtained.

3.3.2 Segmentation using Probabilistic Atlas

For this segmentation, unlike the previous segmentation approach, the only information used to segment the image is the spatial information of the pixels. Before segmenting the image, as explained in subsection I, we registered the probabilistic atlas, which was computed in the previous lab, to each of the images in the dataset. Then, similarly to the previous step, values 1, 2, and 3 were assigned to WM, GM, and CSF, respectively, for each pixel of the image, based on the highest probability across the three tissue types. The formula used is as follows:

$$\text{Segmentation} = \arg \max_{l \in \{1,2,3\}} \text{Prob}[i, j, k, t] \quad \text{for each } (i, j, k) \tag{2}$$

where:

- i, j, k are the indices representing the spatial dimensions (x, y, z) of the image.
- t is the index representing the different tissue types in the fourth dimension of the Probabilistic Atlas.

After computing this formula, the image tissue segmentation is acquired.

3.3.3 Segmentation using both approaches

After computing the previous segmentations, in which we used intensity information and spatial information independently, we have computed a final approach consisting of a combination of both of them. To perform this combination, we have utilised the tissue models to create an image of in- tensity probabilities. Subsequently, we have multiplied the intensity probability image by the probabilistic atlas. As a re- sult, a 4D image with the probabilities of each of the tissues is created. Then, as a last step, following the same methodology, values 1, 2, and 3 were assigned to WM, GM, and CSF, respectively, for each pixel of the image, based on the highest probability across the three tissue types. The formula explaining this entire process is as follows:

- Compute segmentation for each tissue:

$$\text{intensityProb}_t = \sum_{i=0}^{255} \text{tissueModels}_{i,t} \cdot I_{\text{image}=i} \tag{3}$$

- Multiply by Probabilistic Atlas:

$$\text{probImage}_t = \text{intensityProb}_t \cdot \text{atlasProb}_t \tag{4}$$

- Finally, determine the segmentation:

$$\text{finalSeg}_{x,y,z} = \arg \max_{t \in \{1,2,3\}} \text{probImage}[x, y, z, t] \tag{5}$$

where

- $\text{tissueModels}_{i,t}$ represents the probability value for intensity level i and tissue type t.
- $I_{\text{image}=i}$ is an indicator function that is 1 where the image intensity is i and 0 elsewhere.
- atlasProb_t is the probabilistic atlas for tissue t.
- $\text{finalSeg}_{x,y,z}$ is the final segmentation label for voxel (x, y, z).

3.4 Segmentation with GMM

3.4.1 Improvements in GMM computation

In comparison to the last implementation of the Gaussian Mixture Model, multiple changes have been made. Firstly, redundant calculations have been removed. Secondly, the convergence criteria have been adapted to allow for faster convergence with similar robustness. The new convergence criteria can be seen in Equation 6:

$$|\log(\phi_{t+1}) - \log(\phi_t)| < \epsilon \tag{6}$$

where

$$\phi = \frac{1}{N} \sum_{i=1}^{N} p_i(x|\theta) \tag{7}$$

with

- $p(x|\theta)$: Probability density function
- θ: Parameters of the model
- N: Number of pixels

In this formula, the value ϵ was chosen empirically as 10^{-6}. Additionally, if no convergence is reached after 500 iterations the algorithm is stopped. Thirdly, and most importantly, the computation of the probability density function has been changed. More specifically, the computation of the Mahalanobis distance has been adapted after [3] using the Cholesky decomposition, allowing for faster computation. The Cholesky decomposition of the covariance Σ is given by Equation 8:

$$\Sigma = LL^T \tag{8}$$

The computation of the Mahalanobis distance can be changed to Equation 9:

$$x\Sigma^{-1}x^T = x(LL^T)^{-1}x^T = (L^{-1}x)^2 \tag{9}$$

where:

- x: data
- L: Lower triangular Cholesky decomposition

3.4.2 Initialization Methods

Four different initialization methods are available:

- K-means
- Tissue Model
- Probabilistic Atlas
- Probabilistic Atlas and Tissue Model

While the first two are used to initialise the means, the probabilistic atlas is used to initialise the membership weights. This allows the computation of one maximisation step inbetween, resulting in updated covariance, means, mixture weights, and membership weights. In the last method, the means of the tissue model and the covariance, mixture, and membership weights of the atlas are used.

3.4.3 Integration of the Probabilistic atlas

The atlas integration into the segmentation process can occur at various stages: prior to, during, or after the Gaussian Mixture Model computation. When added afterwards, it involves multiplying the atlas probabilities with the membership weights. When used during the computation, the atlas probabilities are multiplied by the membership weights in every iteration; after the expectation step.

4 Results

4.1 Metrics

To evaluate the effectiveness of our approach and analyse the laboratory experiments, we assessed the various cases in our dataset using two key metrics: the Dice Score (DSC), as outlined in Equation 10, and the Balanced Accuracy (BA), which is presented in Equation 11:

$$DSC = \frac{2 \times TP}{2 \times TP + FP + FN} \tag{10}$$

Balanced Accuracy is calculated as shown in Equation (11):

$$\text{Balanced Accuracy} = \frac{\text{Specificity} + \text{Sensitivity}}{2} \tag{11}$$

Both the mean and standard deviation were calculated during the tests in order to enhance the available information and afterwards analyze the data in a comprehensive manner.

4.2 Experiments

In this section, the results of the experiments performed are shown. The results will be split into multiple parts. Figure 06 shows the comparison between single methods; using only EM, Tissue Models (TM) and Label Propagation (LP). Figure 07 demonstrates the comparison of dice scores across methods combining two methods; EM+LP, EM+TM, EM+TM+LP and TM+LP. Finally, Figure 08 shows the comparison of scores combining EM with K-means initialization and integrating a aposteriori of LP and TM responsibilities.

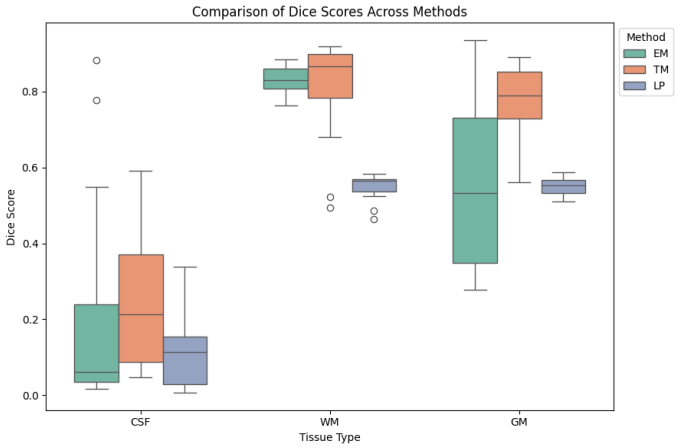

Figure 6: Comparison of the dice obtained for each of the approaches and tissues.

Finally, Figure 09 shows the comparison of mean dice scores of all the approaches.

5 Discussion

In this section, the different results of this project will be discussed and compared to each other.

5.1 Quantitative Results

The analysis of the quantitative results indicates that the EM+KMeans+LP+TM (Freq=1) strategy achieves the best overall performance among the evaluated approaches. This method consistently outperforms others in terms of Dice

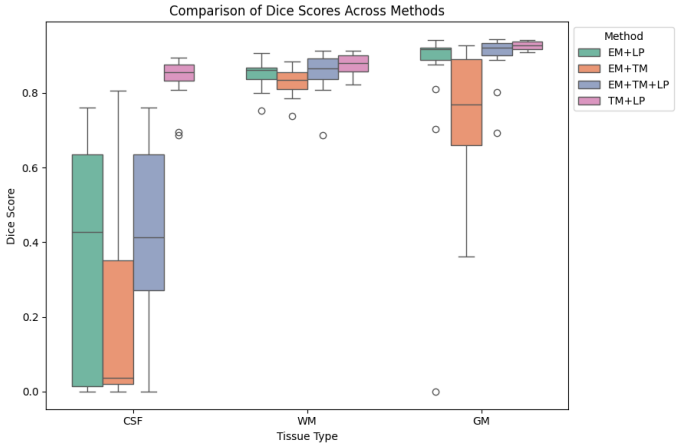

Figure 7: Comparison of Dice Scores Obtained for CSF, WM, and GM Using Different Methods

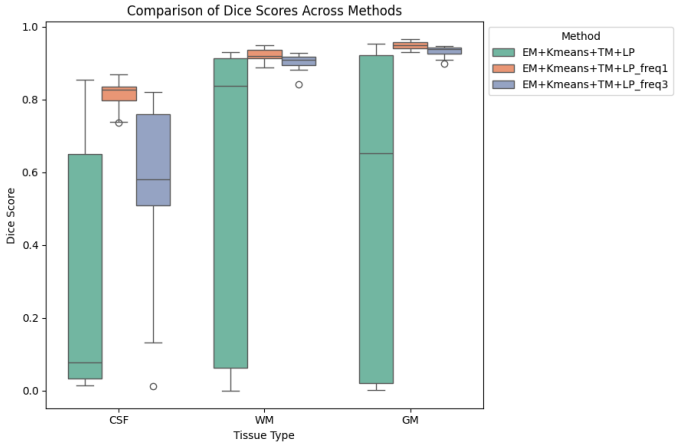

Figure 8: Comparison of Dice Scores for CSF, WM, and GM Using EM+KMeans+TM+LP with Frequencies 1 and 3.

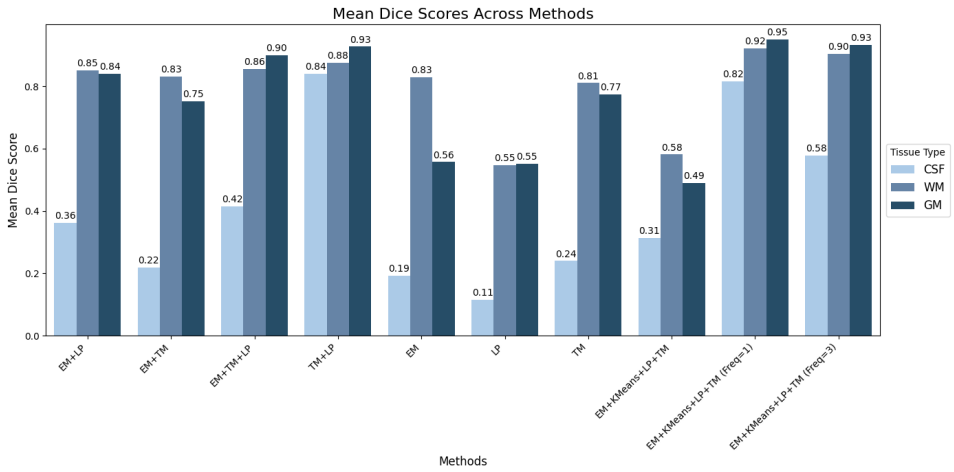

Figure 9: Comparison of the mean dice scores obtained for all of the approaches.

similarity scores across all tissue types. Specifically, it yields the highest Dice scores for CSF (0.815), WM (0.922), and GM (0.950), resulting in the highest average Dice score of 0.896. These results demonstrate the superior capability of the EM+KMeans+LP+TM (Freq=1) strategy to accurately segment all tissue types, highlighting its robustness and effectiveness compared to the alternative methods.

Method	CSF	WM	GM	Average
EM+LP	0.3617	0.8512	0.8407	0.6845
EM+TM	0.2187	0.8303	0.7513	0.6001
EM+TM+LP	0.4152	0.8551	0.9002	0.7235
TM+LP	0.8392	0.8785	0.9269	0.8061
EM	0.1927	0.8286	0.5567	0.5260
LP	0.1150	0.5475	0.5514	0.4047
TM	0.2394	0.8104	0.7736	0.6078
EM+KMeans+LP+TM	0.3136	0.5809	0.4897	0.4614
EM+KMeans+LP+TM (Freq=1)	0.8154	0.9219	0.9502	0.8958
EM+KMeans+LP+TM (Freq=3)	0.5772	0.9043	0.9321	0.8045

Table 1: Mean Dice Scores for CSF, WM, GM, and Overall Average Across Methods

5.2 Qualitative Results

Qualitative Result of the two best performing models are given in Figure 10 and Figure 11.

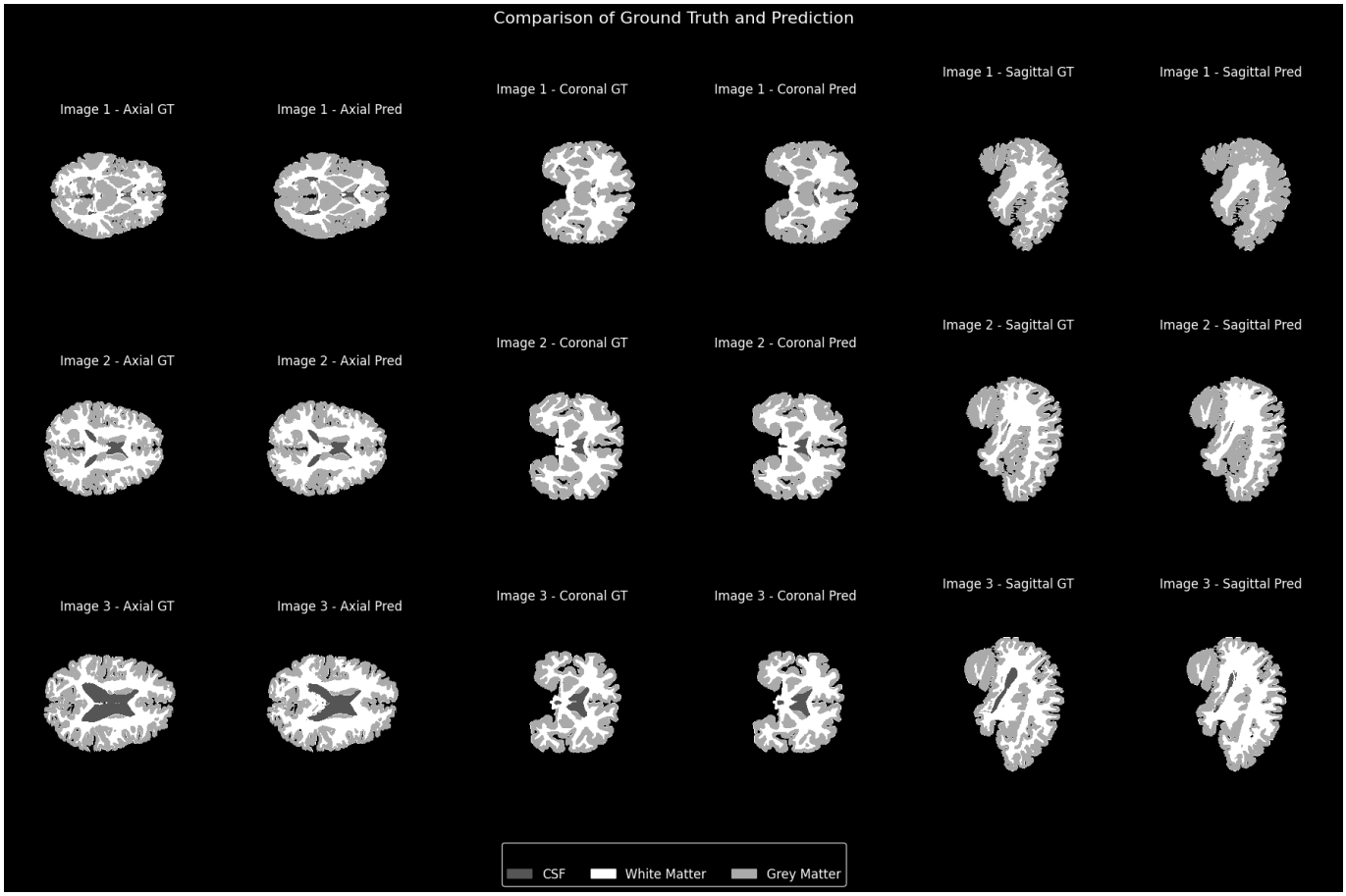

Figure 10: Segmentation results: TM+LP.

5.3 Initialization Comparison

Figure 9 shows the initialization strategy that performed better is the EM+TM+LP with the highest dice score across CSF (0.42), WM (0.86), and GM (0.90). The second-best performance is from the EM+LP strategy that has the dice score of CSF (0.36), WM (0.85), and GM (0.84). In contrast, EM+TM performs relatively poorly, with an average Dice score of 0.600 and significantly lower scores for CSF (0.22), WM (0.83), and GM (0.75), indicating

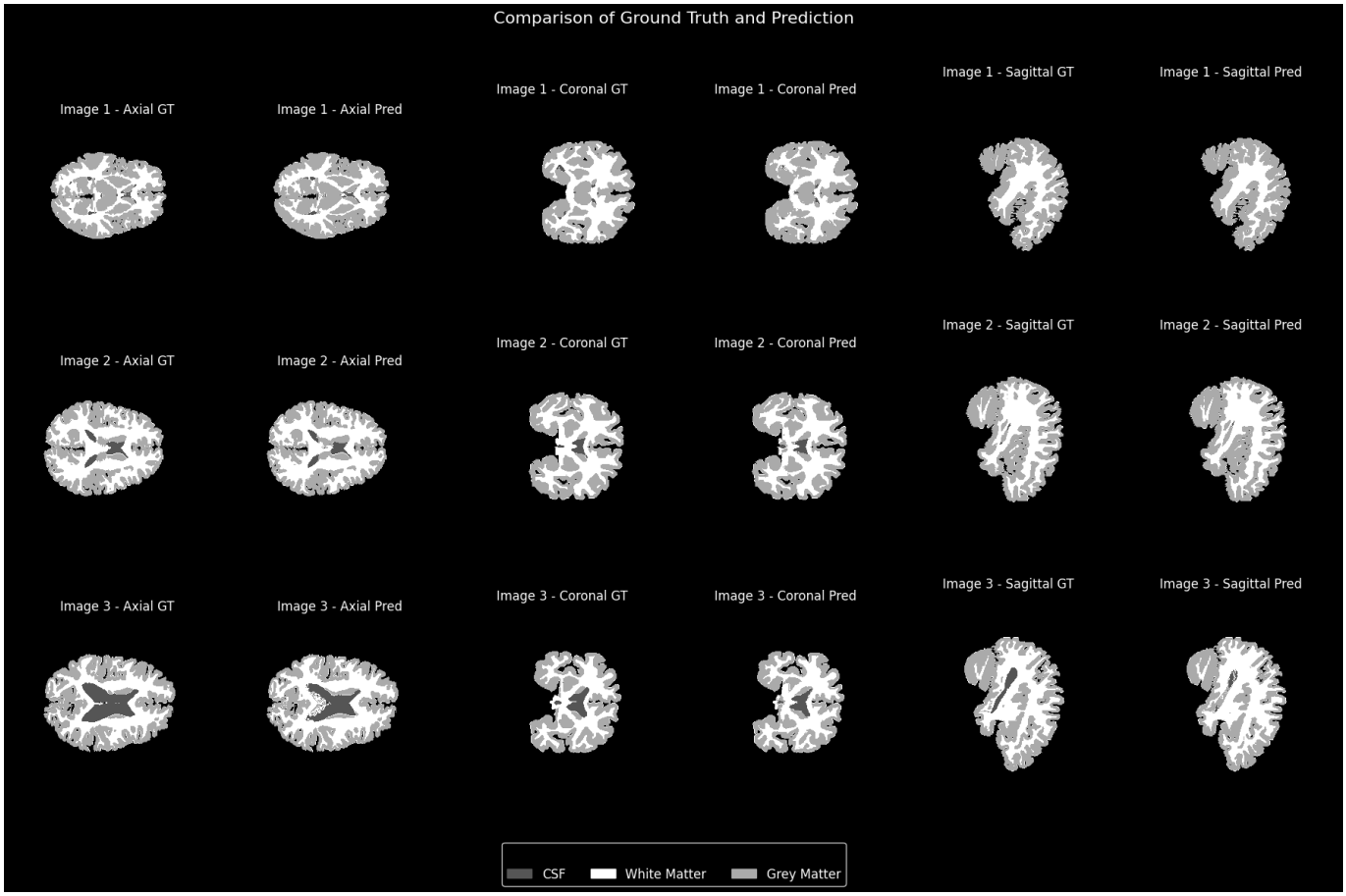

Figure 11: Segmentation results: EM+Kmeans with TM+LP aposteriori inside loop.

that TM initialization alone is less effective. The standalone EM approach shows the weakest performance, with an average Dice score of 0.526 and scores of 0.19 (CSF), 0.83 (WM), and 0.56 (GM). These results clearly establish that EM+TM+LP is the most effective initialization strategy, while EM+LP provides benefits, especially for WM though it does not surpass the performance of EM+TM+LP.

5.4 Inclusion of Spatial Information

Inclusion of spatial information noticeably improves the performance. The approaches without spatial information; EM+TM and only EM demonstrates poor dice score across CSF(0.22), WM (0.83) GM (0.75) and 0.19 (CSF), 0.83 (WM), and 0.56 (GM) respectively. In contrast, the inclusion of LP significantly improves the dice scores particularly in case of CSF because the intensity information is very less and the inclusion of spatial information resulted to a higher dice score compared to the other approaches across across CSF (0.42), WM (0.86), and GM (0.90) with EM+TM+LP and CSF (0.36), WM (0.85), and GM (0.84) with EM+LP.

5.5 Effect of Model Performance on Tissue Types

Figure 5 shows that the model performed poorly in case of CSF tissue type because the intensity value is less for which it get confused with grey matter (GM). Moreover, CSF is a minority class surrounding only a small region in the brain. The overall dice score of CSF is very low compared to WM and GM.

6 References

1. Stefan Klein et al. “elastix: A Toolbox for Intensity-Based Medical Image Registration.” In: *IEEE Transactions on Medical Imaging* **29.1** (2010), pp. 196–205. **DOI:** 10.1109/TMI.2009.2035616.

2. Inge A. Mulder et al. “Automated Ischemic Lesion Segmentation in MRI Mouse Brain Data after Transient Middle Cerebral Artery Occlusion.” In: *Frontiers in Neuroinformatics* **11** (2017). ISSN: 1662-5196. **DOI:** 10.3389/fninf.2017.00003. **URL:** https://www.frontiersin.org/articles/10.3389/fninf.2017.00003.